Active Filtering of Physiological Motion in Robotized Surgery Using Predictive Control

Regular paper

Romuald Ginhoux, *Student member, IEEE,* Jacques Gangloff, *Member, IEEE,* Michel de Mathelin, *Senior member, IEEE,* Luc Soler, Mara M. Arenas Sanchez, and Jacques Marescaux

***Abstract*— This paper presents a predictive control approach to active mechanical filtering of complex, periodic motions of organs induced by respiration or heart beating in robotized surgery. Two different predictive control schemes are proposed for the compensation of respiratory motions or cardiac motions.**

For respiratory motions, the periodic property of the disturbance has been included into the input-output model of the controlled system so as to have the robotic system learn and anticipate perturbation motions. A new cost function is proposed for the unconstrained generalized predictive controller (GPC) where reference tracking is decoupled from the rejection of predictable periodic motions.

Cardiac motions are more complex since they are the combination of two periodic non-harmonic components. An adaptive disturbance predictor is proposed which outputs future predicted disturbance values. These predicted values are used to anticipate the disturbance by using the predictive feature of a regular GPC.

Experimental results are presented on a laboratory testbed and *in vivo* on pigs. They demonstrate the effectiveness of the two proposed methods to compensate complex physiological motion.

***Index Terms*— Medical robotics, Visual servoing, Predictive control, Disturbance rejection.**

I. Introduction

THERE are two main sources of physiological motion inside the body: respiration and heartbeat. Respiration is the most important source of disturbances. It yields large cyclic displacements of several organs, mainly in the abdomen and in the chest. Disturbances induced by the heart are restricted to a small area surrounding it.

These motions can be very disturbing for the surgeon during the operation especially for surgical procedures requiring good precision (*e.g.*, needle insertion and suturing). To overcome this problem some strategies have been developed. Since respiration is controlled by an external ventilator, it is possible to stop it for a short period of time required to perform a very precise gesture. But the limitation of such a technique is obvious: only quick gestures that are deterministic in time can be performed this way.

In cardiac surgery, the heart can be stabilized with a mechanical device [1], [2] that constrains the motions of a small area on its surface by suction or pressure. Despite many improvements since the first version in 1990, stabilizers have still some drawbacks: there is always a remaining residual motion, the suction device may produce injuries to the myocardium and the pressure device is not well suited for operations which are located behind the heart. So, in most cases, the heart has to be stopped and the blood circulation bypassed through an external heart-lung machine which implies more risks and a longer recovery time for the patient.

These are current solutions to work around the problem of physiological motion. Robotic surgery offers a new means to efficiently reject such disturbances with lower risks and better accuracy.

Many contributions deal with physiological motion compensation. Some of them focus their interest more specifically on signal analysis.

The reference [3] is a good survey on human hepatic motion due to respiration. The authors summarize all the reported characteristics of this motion that they found in various medical publications. They also list some therapeutic procedures that could be improved with the use of a filtering system. These procedures mainly involve percutaneous needle placement using ultrasound (US), computed tomography (CT) or magnetic resonance imaging (MRI) guidance.

Anticipating and predicting is a leitmotiv in almost all the works existing on this topic. Indeed, the key idea is to use the repetitive property of physiological motion to anticipate the next disturbance cycle by assuming that it will be almost the same than the previous one which has been learned.

In [4], Ortmaier studies the visual tracking of natural landmarks on the surface of the heart. He uses a motion prediction approach that robustly tracks the features even with disturbances or short occlusions. The goal of this work is to compensate for these motions by using a robotic arm controlled by visual servoing. Robust tracking of heart movements in the image has been successfully completed in this work, but active motion compensation is presented as future work.

In [5], Thakral *et al.* analyze the motion of the chest wall and the heart wall of an anesthetized rat using a fiber optic probe. They point out the complexity of these motions since they result from the addition of two components: one due to respiration and the other due to cardiac beating. In order to model this motion, they use a two-stage adaptive algorithm. In a first stage the Fourier coefficients of the respiratory motion are estimated. Then this component is subtracted from the

R. Ginhoux, J. Gangloff and M. de Mathelin are with the LSIIT (UMR CNRS 7005), University of Strasbourg, Bd Sébastien Brant, F-67400, Illkirch, France

L. Soler, M. Arenas Sanchez and J. Marescaux are with the IRCAD/EITS, Strasbourg University hospital, Hôpital civil, BP426, F-67091, Strasbourg, France

J. Gangloff (jacques@eavr.u-strasbg.fr) is the corresponding author.

initial signal. A second stage estimates the Fourier coefficients of the cardiac disturbance from the resulting signal. In our work, we use a similar approach to estimate the motion of a pig's heart.

The same adaptive algorithm is used in [6] and [7] to model physiological tremor of the surgeon's hand. Only one stage is required since this motion contains only one quasi-periodic component. This work is very original since the disturbance estimator is used in a control loop that cancels the tremor thanks to a piezoelectric actuator.

Few papers actually mention successful experiments with a closed control loop involving a disturbance observer. For this reason the paper [8] from Schweikard *et al.* is very interesting since they describe a radiation therapy system including a radiation source mounted on a robot which tracks a moving tumor. They use the combination of two kind of sensors – a pair of X-ray cameras and an infrared tracking system – to compute a deformation model which describes the correlation between the motion of internal gold markers and external infrared markers. This model is used to obtain the positions of the internal gold markers attached to the target organ with a high refresh rate (60 Hz) even with a very slow X-ray imaging system (0.1 Hz). Then, this measurement is used to control the robot which compensates for the respiration-induced motion of the tumor. However, this work is not focused on the control strategy: for example, the controller might use the deformation model to anticipate the disturbance and reduce the tracking error which is still significant.

In [9], Nakamura *et al.* report a very impressive high-speed visual servoing experiment which uses a small 4 degrees of freedom robotic finger to track a marker attached to the surface of the heart. They demonstrate the feasibility of robotic tracking of fast heart movements and introduce the notion of "Heartbeat synchronization". This defines a control architecture where the surgeon can teleoperate a robot which is synchronized with the heart's motion. Furthermore, the image of the operating scene is filtered to compensate for the motion of the heart. This gives the surgeon the feeling that he is operating on a stopped heart. But in this work, like in [8], the model of the disturbance is not used to improve the tracking.

In this paper, we study the problem from the automatic control point of view. We propose two different solutions, each suited for one kind of physiological motion. For the respiration, we modified the Generalized Predictive Controller (GPC) [10] to add repetitive properties. This repetitive GPC (R-GPC) is able to learn the disturbance cycle due to respiratory motions and so better reject it due to its predictive capabilities. As mentioned before, the heart motion is more complex. We use an adaptive disturbance predictor in combination with a standard GPC to efficiently reject this motion by using the prediction of the disturbance. In our experiments, we use visual feedback to track physiological motion in the image of a camera thanks to standard image-based visual servoing techniques [11], [12].

This paper is divided in five sections. In section II we present the global context of active filtering of physiological motion. Section III is focused on the cancellation of respiratory motions whereas section IV treats the problem of cardiac motions.

II. Active filtering of physiological motion

The aim of active filtering in robotized surgery is to give the surgeon the feeling that he is operating on a scene that is almost still so he can concentrate his efforts only on the useful tasks. Figure 1 gives an overview of such a system.

We assume that the surgical robots are tele-operated. The reference signals coming from the control console are fed to a controller. The controller uses the visual feedback (coming from an endoscope, an external camera, or even from a high-speed CT or US imaging system) to reject the disturbances due to physiological motion while guaranteeing fast and accurate following of the reference.

Disturbance canceling acts on the relative position of the surgical tools with respect to the organs and on the endoscopic view provided to the surgeon. The first is achieved by adding a component to the motion of the surgical tools that is synchronized with the motion of the organ. The stabilization of the image can be obtained either with pure image processing either by moving the vision system. We extend here the concept of "Heartbeat synchronization" from Nakamura *et al.* to the respiration. Furthermore, they only mention software stabilization of the image. A better result can be obtained by moving directly the imaging system, making it follow the moving scene. Such an active mechanical filtering of the image avoids some motion blur effects and maximizes the field of view.

Motions due to respiration and cardiac beating are very different. We discuss here the main properties of these two kind of signals.

A. Respiratory motions

We suppose that the patient is anesthetized and placed under artificial ventilation. The ventilator is a mechanical device that controls the air flow into the patient's lungs thanks to endotracheal intubation. So, since the respiration is forced by this machine, its cycle is perfectly periodical.

The plot (A) in figure 2 gives the measured distance between the tip of a laparoscopic instrument and the surface of an anesthetized pig's liver with respect to time. This measurement was estimated from the endoscopic image with a reconstruction method described in [13]. In this experiment, the instrument is static so the variation of the distance is only due to the motion of the liver. The plot shows clearly that the disturbance due to respiration is periodical. In order to quantify how constant is the disturbance cycle from one period to another, we have processed the signal in plot (A) with the FIR filter $F(z) = 1 - z^{-T}$. The integer T is equal to the number of sampling intervals in one disturbance cycle ($T = 105$ in this case and the sampling frequency is 25 Hz).

This filter cuts all the harmonics of the disturbance (including the first). It simply gives the difference between two consecutive cycles of the disturbance, yielding zero if the signal is perfectly periodical. So the interpretation of the plot (B) in figure 2 is the following: the difference between two consecutive cycles lies in an interval from -1 to 1 millimeters.

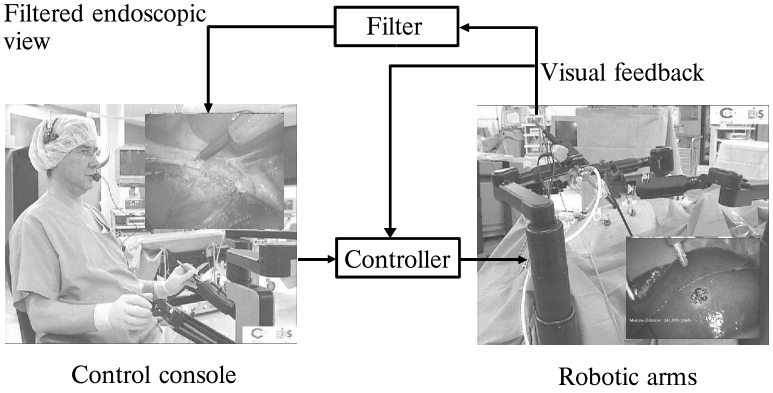

Fig. 1. System overview

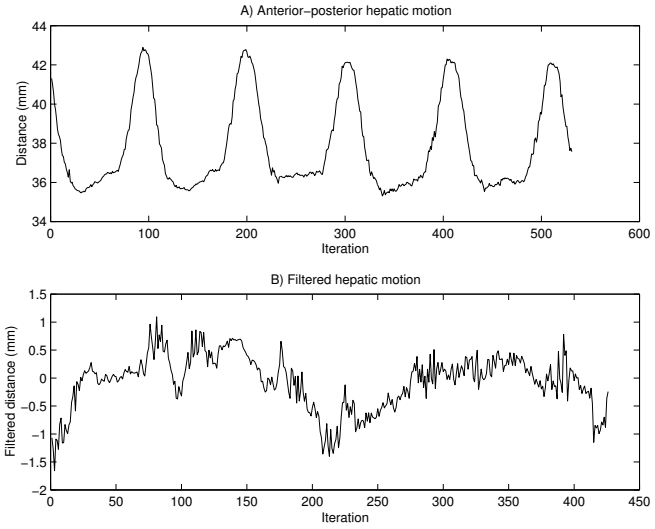

Fig. 2. Measurement of the motion of a pig's liver secondary to respiration

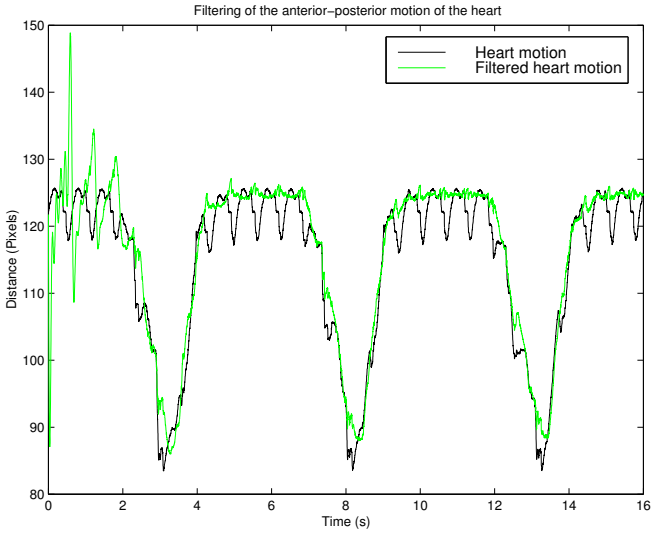

Fig. 3. Disturbance due to cardiac beating. Result of adaptive filtering.

Since the amplitude of the disturbance is about 8 mm, the maximum variation between two cycles is about 12.5%.

So the main property of the disturbance signal due to respiration is its almost-perfect periodicity. Furthermore, it is rather a slowly-varying signal, so that a sampling frequency of 25 Hz is sufficient to avoid aliasing.

B. Cardiac motions

Cardiac motions are much more complex than motions due to respiration since they are the combination of two components as shown in figure 3. These measurements have been acquired with a 500 Hz camera on a living pig and give the anterior-posterior motion of the heart in pixels. In this experiment, the pixel/distance ratio is about 40 pixels/cm. One can see clearly two components in this signal: the component due to the beating of the heart at 1.6 Hz and the component due to the respiration at 0.2 Hz.

The plot shows also that the motion induced by the beating has some very fast transients. Figure 4 is focused on these transients. It shows what would be the result of a sampling at standard video rate, *i.e.* 25 Hz. The lost of information due to aliasing is obvious. So, a high sampling frequency

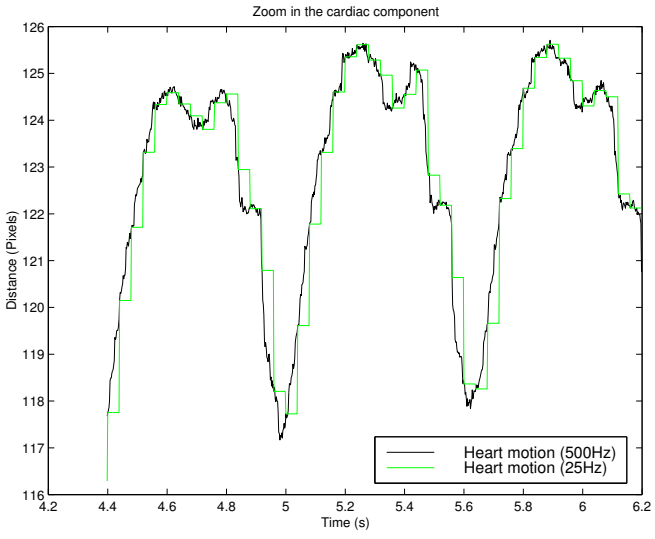

Fig. 4. Details of the cardiac component

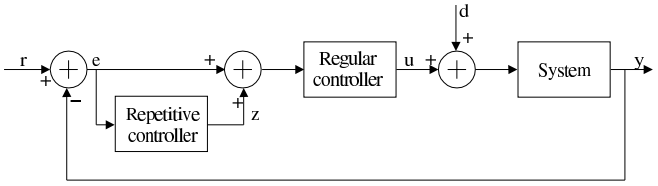

Fig. 5. Typical repetitive control scheme

(greater than 100 Hz) is required for the servo loop that will compensate for these motions.

In the two following sections we will present two different approaches to physiological motion filtering: one suited for respiratory motions and another suited for cardiac motions.

III. Canceling of respiratory motions

Repetitive control is known to work only when the disturbance shape and period is very stable. This is clearly the case with disturbances secondary to respiration.

A. Repetitive control

The idea of *repetitive control* or *iterative learning control* which is very similar was introduced in 1984 (see *e.g.* [14] for a robotic application). The typical scheme of such a control loop is given by figure 5.

A strong assumption is made on the reference since it should be periodical or at least slowly varying. A fast, non periodical, variation of the reference yield an error e that is learned by the repetitive controller and considered as periodical. So, at the next period, the repetitive controller try to anticipate a variation of the reference that does not happen. This yield an overshoot on the output y that is repeated periodically and which amplitude decreases over time according to the forgetting factor of the repetitive controller.

In the context of telemanipulated robotic surgery, the reference r is given by the joysticks of the control console and the disturbance d models the effect of physiological motion on the visual servo loop. To simplify the problem, imagine that the surgeon's joystick controls only the distance between the tip of the instrument and the surface of the target organ (see figure 6). Let y be this distance estimated by vision, r be the reference for this distance given by the surgeon and d be the disturbance added to this distance due to respiration. Since d is periodical and the repetitive controller is tuned to that particular period, the disturbance should be perfectly rejected after a short learning phase. But there is no guarantee that the reference r will be periodical or even slowly varying since it reflects the motion of the surgeon's hand. This is the main drawback that prevents the use of standard repetitive control in this case. To overcome this issue, we propose a modified version of the Generalized Predictive Controller that we called R-GPC and where the reference following function is clearly separated from the periodical disturbance rejection function. With this controller, there is no assumption made on the reference like with standard repetitive control. Furthermore, it is possible to tune separately the reference following performance and the disturbance rejection performance.

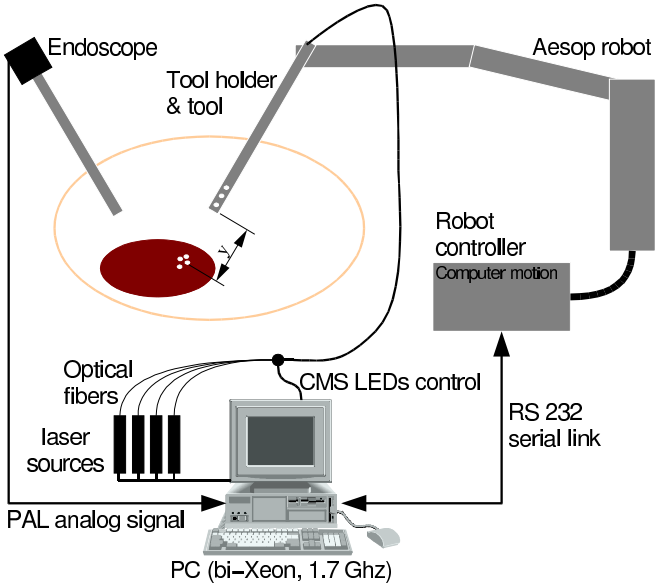

Fig. 6. Cancellation of respiratory motions: experimental setup

B. R-GPC

This section introduces a new unconstrained Generalized Predictive Control scheme based on a repetitive input-output model of the system to be controlled.

Several applications of Model Predictive Control (MPC) to the rejection of periodic disturbances can be found in the literature (*e.g.* in the chemical industry [15]–[17] among others). The controllers are developed using the state-space formulation of MPC and only steady-state control is considered. Thus, no distinction is made between a periodic output disturbance or a periodically varying reference.

Here, we compute separate contributions of the control input to reference trajectory tracking and fast disturbance rejection by means of a new cost function that ensures no interaction between both components.

1) Repetitive ARIMAX model: Unconstrained GPC was originally introduced by Clarke [10], where the system model is represented by an ARIMAX equation,

$$A(q^{-1})y(t) \quad = \quad B(q^{-1})u(t-1) + \frac{C(q^{-1})}{\Delta(q^{-1})}\xi(t) \quad (1)$$

where q^{-1} is the backward operator, $T_s = 1\,s$ is the (normalized) sampling period, A and B are two polynomials modeling the system dynamics (B may also include pure delays), and polynomial C is used to color the zero-mean white noise ξ(t).

Polynomial Δ is used to make noise ξ/Δ be non-stationary, which is suitable to model any perturbation in a control loop [18]. For instance, Δ is set to a pure integrator,

$$\Delta(q^{-1}) = \delta(q^{-1}) \triangleq (1 - q^{-1}),$$

when disturbances are only supposed to be constant steps [10], [18].

However, this classical setting is not appropriate when the actual disturbances vary periodically over time; we therefore propose to modify the ARIMAX model by including repetitive

features of disturbances and write Δ as:

$$\Delta(q^{-1}) = \delta(q^{-1})\,\Delta_R(q^{-1}) \quad (2)$$

$$\text{with } \Delta_R(q^{-1}) \triangleq 1 - \alpha\, q^{-T} \quad (3)$$

and $T \in \mathbb{N}$, $T \geq 2$, is the number of sampling periods in one period T^* of the disturbance. So the perturbation model ξ/Δ is actually made periodic with a period equal to T. The scalar α is chosen in $]0;1]$ and acts as a forgetting factor. Its main effect is to filter the control signal in order to increase the robustness against errors in the system model or noise in the visual measurements.

2) Separation of control input: Writing $y(t)$ in equation (1) as $y(t) = y_{\mathtt{th}}(t) + \epsilon(t)$ yields the two following equations:

$$A\, y_{\mathtt{th}}(t) = B\, u_1(t-1) \quad (4)$$

$$A\, \epsilon(t) = B\, u_2(t-1) + \frac{C}{\Delta}\, \xi(t) \quad (5)$$

where $u(t)$ is now written as $u(t) = u_1(t) + u_2(t)$. The control signal $u_1(t)$ is the input of the theoretical system model (4), yielding the theoretical output measurement $y_{\mathtt{th}}(t)$. The control signal $u_2(t)$ is the part of the total control signal $u(t)$ that is responsible for the rejection of the measurement error $\epsilon(t)$ due to noise and disturbances.

Multiplying equation (4) by δ yields:

$$A\, \delta y_{\mathtt{th}}(t) = B\, \delta u_1(t-1) \quad (6)$$

Substituting $A^{'}$ for $\Delta_R A$ and $B^{'}$ for $\Delta_R B$, the product of equation (5) by Δ yields:

$$A^{'}\, \delta\epsilon(t) = B^{'} \delta u_2(t-1) + C\, \xi(t) \quad (7)$$

Then, following and adapting the method from [10], [18] to this formulation of the controller, the expression of the cost function for the unconstrained R-GPC is derived from equations (6) and (7) as:

$$\begin{aligned}\mathcal{J}(u = u_1 + u_2, k) = &\sum_{j=N_1}^{N_2} \|\hat{y}_{\mathtt{th}}(k+j) - r(k+j)\|^2 \\ &+ \sum_{j=N_1}^{N_2} \|\hat{\epsilon}(k+j)\|^2 + \lambda \sum_{j=1}^{N_3} \|\delta u_1\,(k+j-1)\,\|^2 \\ &+ \mu \sum_{j=1}^{N_3} \|\delta u_2\,(k+j-1)\,\|^2 \end{aligned} \quad (8)$$

where N_1, N_2 are respectively, the lower and upper bound of the cost horizon, and N_3 is the length of the control cost horizon; $N_3 < N_2$ and $\delta u_i(t+j-1) = 0$ for $j > N_3$, $i = 1$ or 2; λ and μ weight the relative importance of both control energies. The reference trajectory is denoted by $r(t)$.

The aim is to compute the N_3 future control increments $\delta u_1(t+j-1)$ and $\delta u_2(t+j-1)$ that minimize the cost function (8). This yields control increments $\delta u_1(t+j-1)$ that minimize the error between the predictions of the theoretical model output and future reference values $r(t+j)$ and control increments $\delta u_2(t+j-1)$ that make the actual system output tend toward the theoretical one, or, equivalently, compensate for the measurement disturbances. Note that the two sets of control increments separately contribute to the minimization of the cost function. As the control law is receding, only the first control increment $\delta u(t) = \delta u_1(t) + \delta u_2(t)$ is sent to the system, and the overall minimization is performed at each time step.

The advantages of this decomposition are several. The control signal u_2 that acts on the disturbance rejection is equivalent to an autonomous mode of the robot since it is independent of control signal u_1 that is directly driven by the surgeon. Different levels of saturation can be put on both control inputs in order to prevent teleoperated component $u_1(t)$ from saturating with no influence on the perturbation cancellation in case of fast changes in the reference signal. It is possible to tune separately the bandwidth of the disturbance rejection and the bandwidth of the reference following thanks to the parameters μ and λ.

C. Laboratory testbed

We have developed a testbed to validate the control strategy in our lab before making *in vivo* experiments (see figure 7 and 8).

1) Description: In this testbed, we use two robots. The robot that holds the simulated instrument has 6 actuated degrees of freedom (DOFs). It has the same kinematics than the Aesop or Zeus arm from Computer Motion™ but with all its joints actuated. Furthermore, the power of the actuators has been increased to achieve high dynamic performances. This robot is a prototype that was manufactured by SINTERS™ from our specifications.

We use another 2-DOF robot to simulate a moving organ. This robot has 2 perpendicular rotational joints. It holds a planar target that simulates the surface of the organ. So the motion of the target can be precisely controlled to make a periodic complex displacement.

The endoscope is simulated by a static camera mounted on a tripod looking at the moving target. It is a high-speed CCD camera (DALSA™ CAD6) that runs at 500 frames per second with a resolution of 256×256 pixels. We chose high-speed imaging to be able to track fast simulated organ motions. Indeed, we want to use the same testbed to validate compensation algorithms for cardiac surgery.

With this system, the whole visual servo loop is synchronized with the image acquisition and so runs at 500 Hz. To guarantee a stable sampling frequency, the use of a real-time system is mandatory. We use RTAI [19]. We developed a customized version of the frame grabber driver (PC-DIG from Coreco Imaging™) that works in real-time mode. So the vision computer (see figure 8) performs image acquisition, image processing and control processing in real-time mode. The control signals are transmitted to the controller of the 6-DOF robot *via* a 10 Mbits/s serial link.

This controller was also custom-developed in our lab. It can be switched in a slave mode where the joint position loops are deactivated and the control signals coming from the serial link are directly sent to the joint-level velocity loops of the robot. In this mode, the controller is synchronized by the vision computer thanks to the serial link, and so, in our case, it sends the control signals at 500 Hz. The delays are drastically

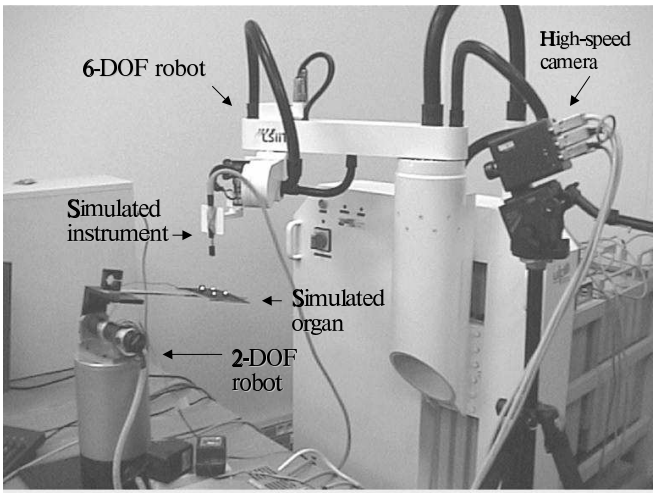

Fig. 7. Picture of the testbed

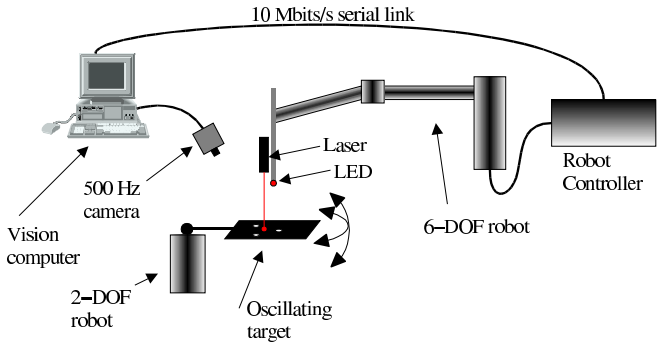

Fig. 8. Testbed diagram

reduced with this scheme: there is only a delay of one sample due to the control signal transmission.

2) Visual measurement: With this testbed the experiment can be easily extended to the compensation of 3 DOFs by simply adding some markers on the oscillating target (see figure 8 and 9). We also use two optical markers to localize the position of the instrument with respect to the target: the position of the instrument's tip is marked by an LED, and a laser source projects a beam parallel to the axis of the instrument, yielding a spot on the surface of the target.

Let M, L and T be 3 points in the image that are respectively the center of mass of the markers on the target,

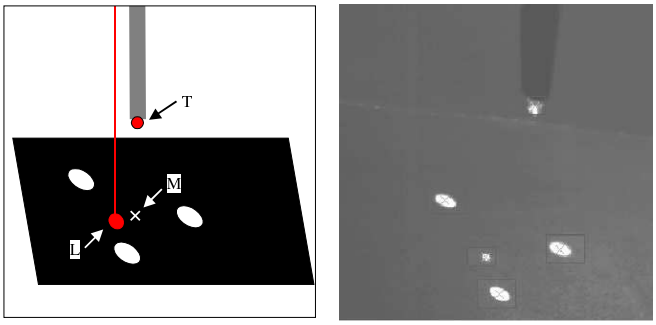

Fig. 9. Image of the 500Hz camera

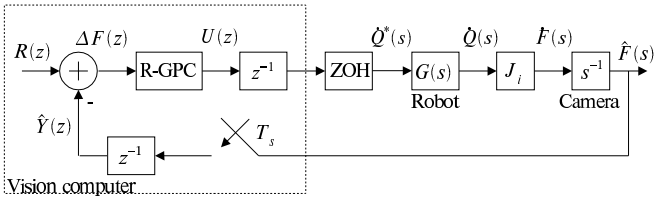

Fig. 10. Block diagram of the linearized visual loop

the center of the laser spot and the center of the LED. Let ${}^cM$, ${}^cL$ and ${}^cT$ be respectively the coordinates of M, L and T in R_c, the image frame: ${}^cM = [x_m \ y_m]^T$, ${}^cL = [x_l \ y_l]^T$ and ${}^cT = [x_t \ y_t]^T$. Three parameters are controlled in the image plane: the coordinates $\Delta x = x_m - xl$ and $\Delta y = y_m - y_l$ of the vector $L\vec{M}$ and the difference $d = y_t - y_l$. Δx and Δy are servoed to zero so that the instrument tracks the target area on the surface of the simulated organ whereas d, the vertical distance in pixels between the tip of the instrument and the surface of the simulated organ is servoed to a specified reference d_0. Let us define $F = [d \ \Delta x \ \Delta y]^T$ the feature vector.

3) Model of the visual loop: In this experiment, we only use the first 3 joints of the robot. Let Q be the vector of the joints' positions: $Q = [q_1 \ q_2 \ q_3]^T$. Since the relative position between the 6-DOF robot and the target cannot be known in advance, the interaction matrix $J_i : \dot{F} = J_i \dot{Q}$ must be identified. In a preliminary phase, a step displacement is performed successively on each of the first 3 joints. The corresponding displacements are measured in the image yielding an estimation of J_i, valid in an area close to the working point.

To perform R-GPC control, it is necessary to have a linear model of the visual loop. The linearized model of the visual loop is given by the block diagram in figure 10. We assume that the dynamic behavior of the robot is almost linear around the working point and so can be modeled by a transfer function $G(s)$. This is a strong assumption when performing direct torque control. But in our case there are joint-level velocity loops that reject nonlinearities like Coriolis, centrifugal, or gravity effects and therefore have a linearizing action on the model (see [20] for more details). The transfer function $G(s)$ is obtained by using standard linear identification techniques.

In the block diagram (figure 10), the feature vector reference $R(z)$ is compared to the feature vector measurement $\hat{Y}(z)$ estimated by vision yielding the vector $\Delta F(z)$ of the errors in the image plane. The R-GPC outputs a control signal $U(z)$ that is sent to the robot controller with a fast serial link (1 sample delay modeled by z^{-1}) and then converted into an analog voltage $\dot{Q}^*(s)$ with a DAC modeled by a zero-order hold (ZOH). Then, $\dot{Q}^*(s)$ is sent as reference to the built-in velocity loops of the joints' power amplifiers.

The relationship between the joint velocity vector $\dot{Q}(s)$ and the image plane velocity vector $\dot{F}(s)$ is J_i, the interaction matrix. Then $\dot{F}(s)$ is integrated (transfer function s^{-1}) yielding $\hat{F}(s)$, the displacement in the image plane estimated by the camera. This information is sampled by the frame grabber at the frequency $1/T_s$. The delay z^{-1} in the feedback loop models the image acquisition and processing duration.

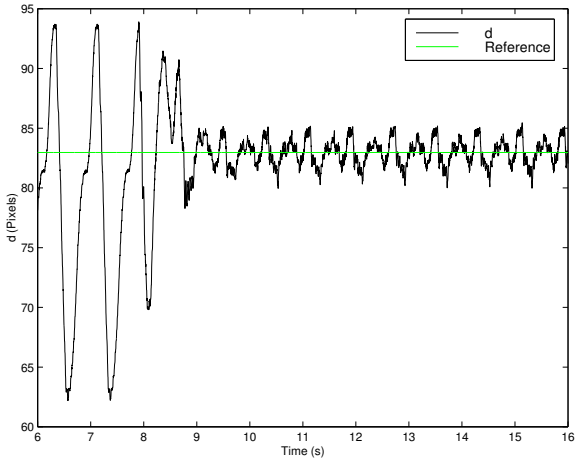

Fig. 11. Testbed: regulation of d with R-GPC

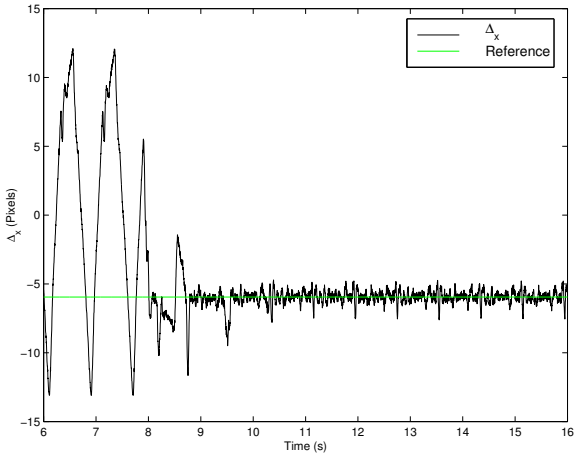

Fig. 12. Testbed: regulation of Δ_x with R-GPC

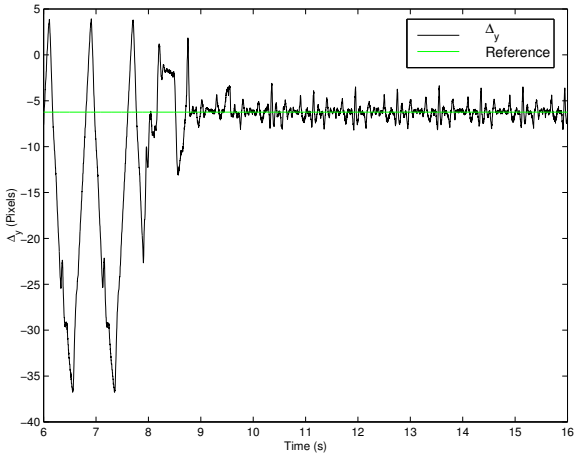

Fig. 13. Testbed: regulation of Δ_y with R-GPC

From this simplified block diagram, we obtain:

$$V(z) = \frac{Y(z)}{U(z)} = z^{-2}(1 - z^{-1})\mathcal{Z}\left\{\frac{J_i G(s)}{s^2}\right\} \qquad (9)$$

where $\mathcal{Z}$ represents the z-transform. So the transfer function $V(z)$ models the linearized dynamic behavior of the visual open loop. It is valid in a small area around the working point. In the particular case of robotized surgery, this assumption is almost always verified since the robot is usually working in a small subspace of its workspace (see [13]). Nevertheless, in the event of larger displacements, a gain scheduling control strategy could be used.

Finally, this transfer function is converted to the ARIMAX form (equation (1)) using well-known regularization techniques. So the gain of the R-GPC computed with this model is optimal with respect to the cost function (8).

D. Experiments

1) Laboratory experiments: For the laboratory experiments[1] we used the testbed described in section III-C to validate the repetitive approach. We simulated the motion due to respiration by programming the controller of the 2-DOF robot to describe a cyclic trajectory.

In figures 11, 12 and 13 the R-GPC was switched on at time $t = 8s$. After approximately one period, the disturbance has been learned and almost perfectly rejected. For these experiments, the pixels/distance ratio is approximately 30 pixels/cm. So, for a disturbance whose peak-to-peak amplitudes for d, Δ_x and Δ_y are respectively 1 cm, 0.8 cm and 1.3 cm, the residual peak-to-peak amplitude of the error with R-GPC is respectively 1.6 mm, 0.8 mm and 1.6 mm. This demonstrates the efficiency of the proposed method.

2) In vivo *experiments:* The experimental setup[2] of the *in vivo* experiment is described in figure 6. It is the same than the one used in [13] except for the unit of the distance y. In this work we use the distance in the image between the tip of the instrument and the surface of the target organ expressed in pixels whereas in [13], the absolute distance in millimeters was reconstructed. For a given working area, there is a linear relationship between these two values. With the vision system that we used (Stryker™ 988), and with the relative position of the instrument with respect to the endoscope that we had in our experiments, the pixel/distance ratio is about 5 pixels/mm. This ratio is identified in an automated sequence prior to visual servoing.

The model of the open loop is slightly different that the one obtained on the testbed. Indeed, the transmission between the vision computer and the controller of the Aesop arm is especially slow yielding 6 additional sample delays in the open loop. The endoscopic system outputs a standard PAL video signal, so the sampling frequency of the visual loop is 25 Hz.

In figures 14 and 15 we compare the response of the system with a standard GPC and a R-GPC. The GPC and the R-GPC are tuned (with parameters λ and μ) to achieve the best trade-off between stability and performance (see [21] for a tutorial about GPC tuning techniques). A step is performed on the reference r to simulate the action of the surgeon. These figures demonstrate clearly the superiority of the repetitive strategy. With the R-GPC, the maximal error is reduced by a factor 2.5 with respect to standard GPC.

[1]See the video at address ftp://eavr.u-strasbg.fr/pub/jacques/simulation.avi
[2]See the video at address ftp://eavr.u-strasbg.fr/pub/jacques/resp.avi

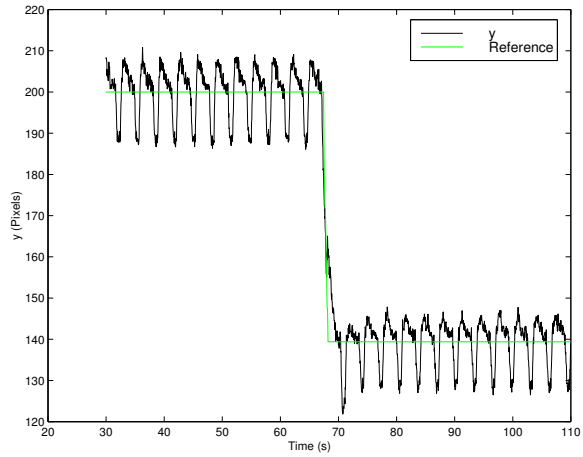

Fig. 14. *In vivo*: regulation of y with GPC

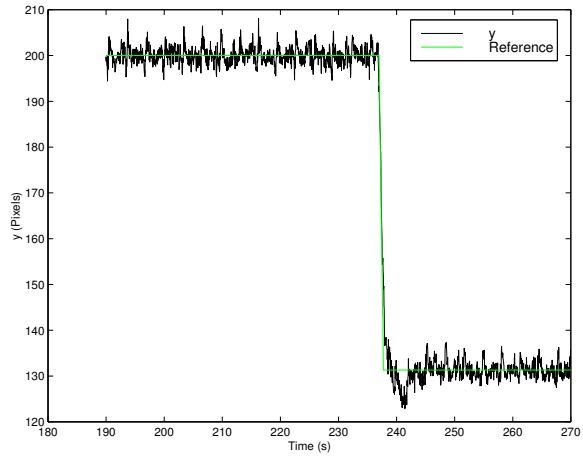

Fig. 15. *In vivo*: regulation of y with R-GPC

Figure 16 shows the decoupling of the two control signals u_1 and u_2: the first contributes only to the following of the reference whereas the latter contributes only to the rejection of the repetitive disturbance.

IV. Canceling of cardiac motions

The repetitive strategy cannot be used here since the motion of the heart is not constituted by one unique period. Instead we use an adaptive disturbance predictor. This predictor is used in combination with a regular GPC to anticipate future motions of the heart yielding a better rejection. We call this control scheme GPC+A where the A stands for Adaptive.

Since the disturbance signal due to cardiac beating has some very sharp edges, a high sampling frequency is mandatory in order to avoid aliasing. This is the main reason why we use a 500 Hz visual feedback. The other reason is linked to the manipulator dynamics. Indeed, to make a high-speed visual servo loop, it is necessary to take into account the dynamics of the manipulator as explained in section III-C.3. To achieve a high bandwidth, the high-frequency modes must be modeled. This is possible only with a high sampling rate, typically greater than 100 Hz for a standard manipulator.

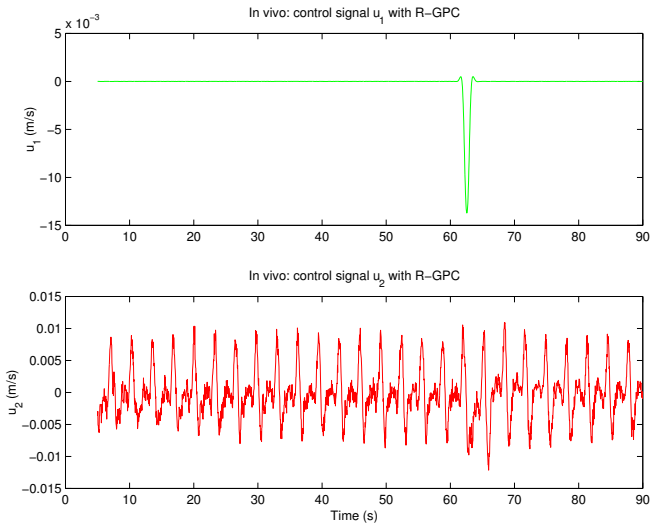

Fig. 16. *In vivo*: control signal u_1 and u_2 with R-GPC

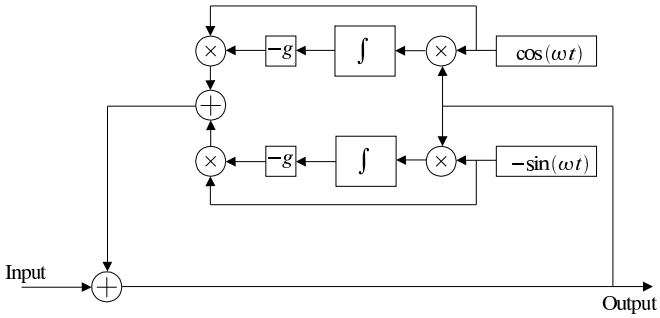

Fig. 17. Adaptive frequency-cancellation filter

A. Adaptive disturbance predictor

The idea is to cancel the cardiac component in the disturbance signal by using a scheme proposed by Bodson *et al.* in [22]. The block diagram of this adaptive frequency-cancellation filter is given in figure 17 where ω is the frequency that must be canceled and g is a positive gain that tunes the velocity of the gradient descent.

Let ω_c be the frequency of the fundamental of the cardiac component. So, by defining $\omega = \omega_c$ in figure 17, the fundamental of the cardiac component is suppressed in the disturbance signal. An analysis of the power spectral density shows that at least the 5 first harmonics should be taken into account. This is possible by simply parallelizing the action of 5 filters, each of them tuned on a specific harmonic (ω_c, $2\omega_c$, ...$5\omega_c$) as shown in figure 18. A similar approach is described in [23].

Figure 3 demonstrates the efficiency of this filter: the input and the output of the filter are drawn on the same plot. It shows clearly that the cardiac component has almost been suppressed from the input signal. Furthermore, one can notice that no delay is added by this filter.

Let S_d be the measured disturbance signal. We would like to predict N_2 future samples $\hat{S}_d(t+1)$, ... , $\hat{S}_d(t+N_2)$ of this signal. The adaptive filter outputs a signal S_r that contains only the respiration component. So $S_c = S_d - S_r$ is a good

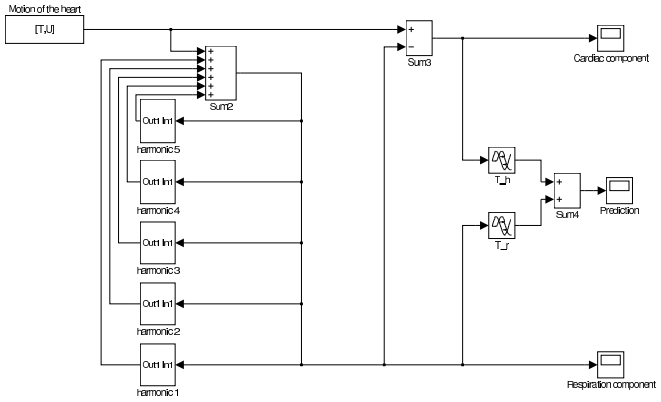

Fig. 18. Adaptive disturbance predictor

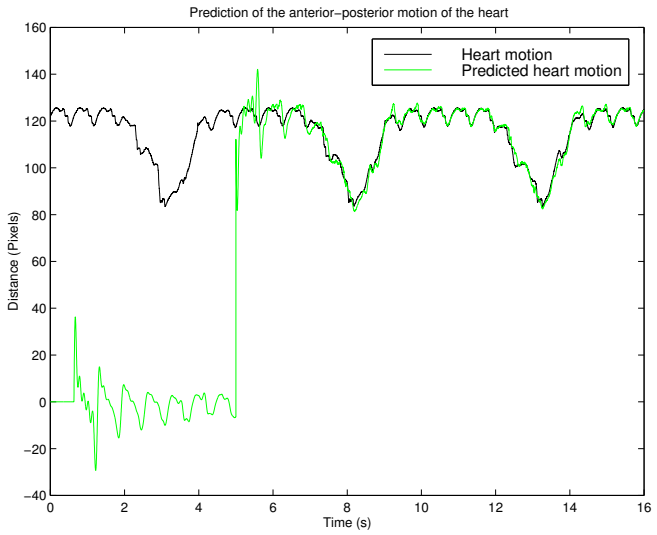

Fig. 19. Prediction of the motion of the heart

estimate of the cardiac component. If we assume that S_r and S_c are periodic with respectively a period T_r and T_c, then $S_r(t) = S_r(t - T_r)$ and $S_c(t) = S_c(t - T_c)$. So, if $N_2 < T_r$ and $N_2 < T_c$, then,

$$\hat{S}_d(t+k) = S_r(t - T_r + k) + S_c(t - T_c + k) \quad \forall k \in [1, N_2] \tag{10}$$

The block diagram of this algorithm is presented in figure 18. Figure 19 compares the predicted value $\hat{S}_d(t)$ obtained from equation (10) with $k = 0$, and the real measured value S_d. It shows that the predictor must learn at least one period of the heart beating and one period of the respiration to anticipate there respective motions. This explains why the output of the predictor is zero for the duration of the heart beating period (up to t=0.625 s) and why the estimation of the full motion of the heart (beating + respiration) starts to fit the real motion at time t=5s (the respiration component is zero for $t \leq 5s$). The plot shows that after a transient of 8 seconds the predictions fit the measurements pretty accurately.

This filtering strategy assumes that the cardiac rhythm is known and steady. This assumption is generally valid on an anesthetized patient. If not, the value of ω_c can be monitored by using the electrocardiogram machine so that the filter can adapt to a slow variation. Alternatively, direct estimation of frequency could be implemented within the multi-harmonic adaptive disturbance predictor, as in [6]. In the rare case of fast and arrhythmic variations of the heart's beating, the prediction error can be used to trigger an emergency procedure.

B. Measurement of the disturbance

The testbed presented in figure 7 and 8 is used to validate this control scheme. The visual servoing is in an *eye-to-hand* configuration which means that the camera is static and looking at the robot end-effector. This particular configuration allows us to easily estimate the disturbance due to the motion of the organ.

Let F be the vector of the visual measurements (see section III-C.2). Let us decompose F in 3 terms: $F = F_0 + S_b + S_d$ where S_b and S_d are respectively the contributions of the robot motion and the organ motion to F and F_0 is the initial value of F. By definition, the interaction matrix J_i is the relationship *without any disturbance* between the motion of the robot joints and the motion in the image valid in a small area around the working point: in this case $\dot{F} = \dot{S}_b = J_i\dot{Q}$ (see section III-C.3).

So, in a first-order approximation, $S_b = J_i(Q - Q_0)$ where Q is the current position of the robot and Q_0 is a position located at the center of the working area (*e.g.* the position of the robot at the start of the visual servoing). We then obtain that $S_d = F - F_0 - J_i(Q - Q_0)$. Notice that S_d estimated this way is the displacement in the image due to the motion of the organ with a static robot staying "virtually" at position Q_0.

C. Visual servo loop

The block diagram of the visual servo loop is given in figure 20. The controller is a standard GPC. There is no repetitive component in the noise model, so $\Delta(q^{-1}) = \delta(q^{-1}) \triangleq (1 - q^{-1})$ (see section III-B.1). Furthermore, there is no more need to split the control signal in two parts like in the R-GPC, so the cost function is given by:

$$\mathcal{J}(u,k) = \sum_{j=N_1}^{N_2} \|\hat{y}(k+j) - r(k+j)\|^2 + \lambda \sum_{j=1}^{N_3} \|\delta u\,(k+j-1)\,\|^2 \tag{11}$$

where the variables have the same definition as in equation (8). The model $V(z)$ of the open loop, and consequently the matrices B and A of the ARIMAX model, are the same as in section III-C.3.

When the disturbance S_d is known in advance, it can be shown (see *e.g.* [18]) that by replacing the original reference $r(k+j)$ by the modified reference $r_m(k+j)$ in the cost function (20) the resulting controller is able to anticipate the disturbance, yielding a smaller error.

The *modified* reference $r_m(k+j)$, $\forall j \in [N_1, N_2]$, is defined by:

$$r_m(k+j) = r(k+j) - (S_d(k+j) - S_d(k)) \tag{12}$$

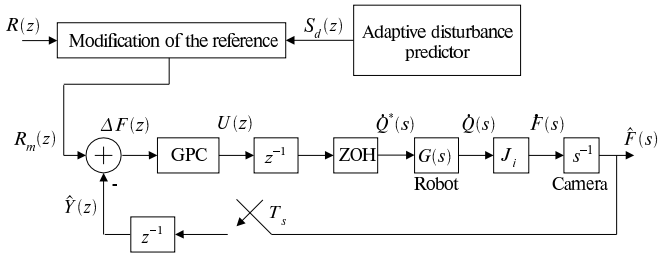

Fig. 20. Visual servo loop of the GPC+A

One can notice that since the future reference values are shifted by a value that is a difference of predicted disturbance values, an offset in the disturbance prediction would have no effect on r_m.

D. Experiments

In this section all the measurements are given in pixels. The pixel/distance ratio depends on the relative position of the camera with respect to the scene. Nevertheless 40 pixels/cm is a good approximation for all 3 coordinates of the feature vector F.

1) Laboratory experiments: To validate our approach we performed first of all some experiments in the laboratory on our testbed since it is obviously much more convenient to develop the code on a simulated heart rather than on a real one. Nevertheless, to accurately simulate the motion of the heart with the oscillating target we acquired with the 500 Hz camera the motion of markers attached on a pig's heart. Then, in our lab, we replayed the acquired sequence with the oscillating target in order to have the most realistic motion possible.

The variations of $F = [d\ \Delta x\ \Delta y]^T$ due to the motion of the oscillating target with no compensation are given in figure 21. One can see that these curves are pretty similar than those acquired in real conditions given in figure 24.

In figure 22, we compare the error in the image with and without modification of the reference. The modification of the reference is switched on at time $t = 12s$ yielding clearly a better rejection for Δ_x and Δ_y. Nevertheless, on d, standard GPC control without anticipation seems to give better results.

This is due to a technical issue: the only joint of the robot that contributes to the variation of d, the vertical distance in the image, is the first one which is a vertical translation. This translational joint is also the heaviest and consequently the slowest. During the experiments, we observed that the control signal sent to this joint often saturated, especially when switching on the modification of the reference. We tried the same experiment with a slower simulated cardiac motion that yields no saturation and we could observe in this case an improvement on d when switching on the modification of the reference.

So the first joint of this robot is too slow to follow the fast transients due to the heart beats. In a future evolution of this experiment, the design of the robotic arm should be re-considered in order to achieve better performance in the vertical direction.

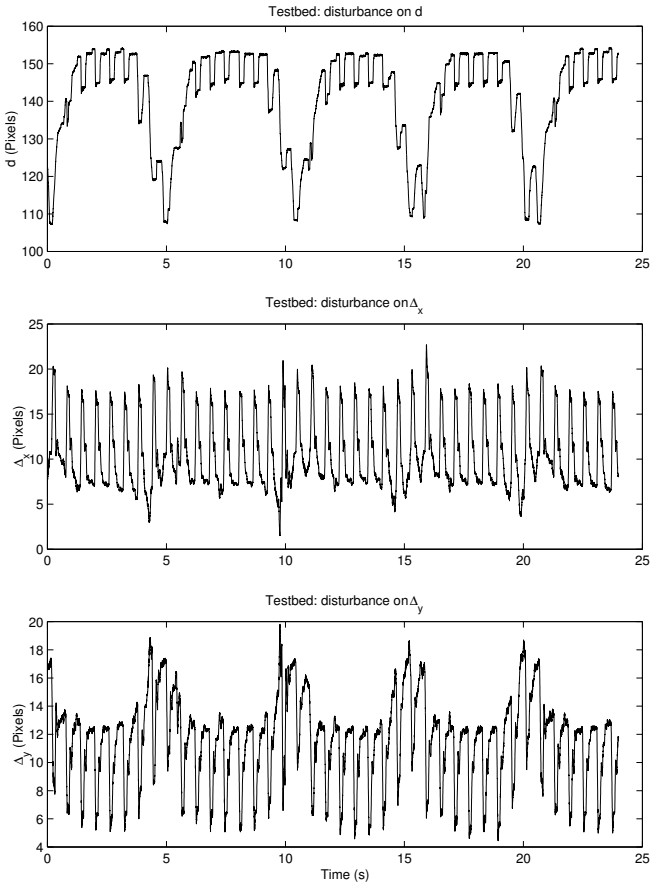

Fig. 21. Testbed: simulated motion of the heart

2) In vivo *experiments:* For the *in vivo* experiments[3], we put some optical markers on the surface of an anesthetized pig's heart as shown in figure 23. An access to the pig's heart was obtained by left anterior thoracotomy. The cardiac frequency is controlled by the injection of drugs, the propofol and the pavulon. There is no difference with the laboratory experiment other than the way of producing the disturbance.

As expected, the *in vivo* experiment confirms the results obtained with the testbed as shown in figure 25. Table I summarizes these results. There is a reduction of 80% for the variance of the disturbance when using a standard GPC. This reduction is respectively 93% and 84% for Δ_x and Δ_y when using the adaptive disturbance predictor in combination with the GPC. These results demonstrate the validity of the proposed method: anticipation of the disturbance yields better rejection.

V. Conclusion

In this paper we tackle the difficult problem of canceling complex physiological motion using a predictive control visual servoing scheme.

We propose two different approaches for motions secondary to respiration and cardiac motions. Indeed, the repetitive control approach is very well-suited to compensate respiratory motions since they are perfectly cyclic due to the external

[3]See the video at address ftp://eavr.u-strasbg.fr/pub/jacques/beating.mpg

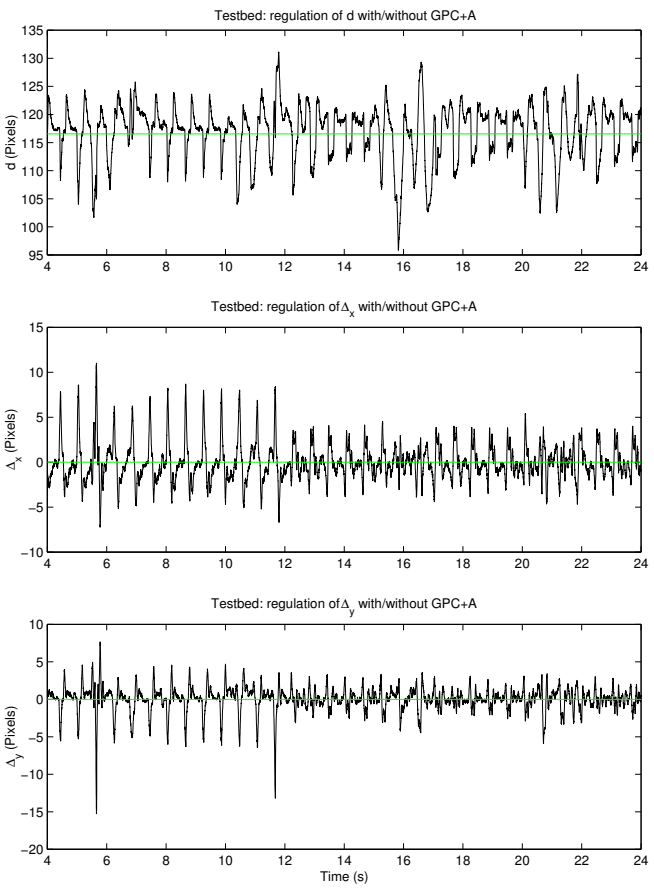

Fig. 22. Testbed: regulation with GPC and GPC+A (at t=12s)

TABLE I
STATISTICAL EVALUATION OF THE MOTION COMPENSATION

Data	Nber of samples		Mean (pixel)	Min. (pixel)	Max. (pixel)	Var. (pixel^2)
S_d	7546	Δ_x	6.97	-5.88	28.58	**80.52**
		Δ_y	-19.24	-31.25	-5.44	**42.20**
GPC	18707	Δ_x	-0.02	-10.55	12.65	**17.58**
		Δ_y	-0.01	-7.34	7.60	**8.57**
GPC+A	5601	Δ_x	0.09	-7.87	7.68	**5.98**
		Δ_y	-0.25	-10.94	7.01	**6.82**

ventilator. Laboratory and *in vivo* experiments validated the proposed approach.

The motion of the heart is much more complex since it is the combination of cardiac beats and motions due to respiration. The frequencies of the two signals are in general non-harmonic, so the repetitive approach cannot be used. Instead, we propose an adaptive disturbance predictor that separates the two components of the disturbance and, using the periodic characteristics of the two extracted signals, outputs predicted values of future disturbance samples. These predicted values are used by a regular GPC to improve the rejection. Both laboratory and *in vivo* experiments validate this predictive approach.

We will concentrate our future work on the improvement

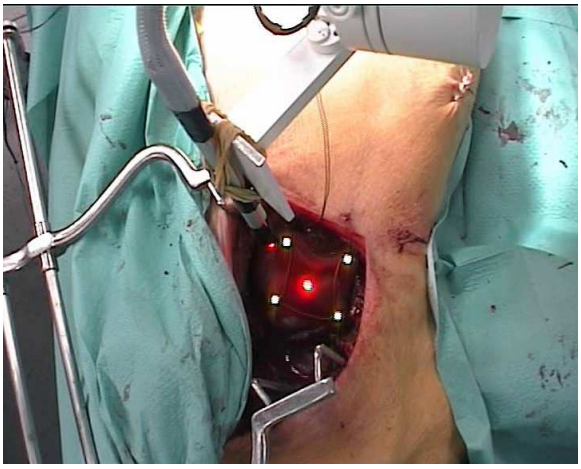

Fig. 23. *In vivo* experiment

of the cardiac motion compensation. We found in our experiments that one joint of the robot is not fast enough to follow the heart beats. So we need to think about a new structure that can be fast and also accurate. Furthermore the results presented were obtained through a large incision, but of course in the long term the work aims toward a keyhole incision, which will represent a fulcrum at the point of entry through the skin, restricting the freedom of motion of the tool. This constraint can be integrated into the control loop *e.g.* by using a force sensor on the robot end-effector that measures the constraints tangential to the skin surface at the entry point. Of course, the wrist joints of the robot should be used to move the tip of the tool but the control strategy would remain the same.

We need also to improve the way of detecting the motion of the heart. The current system constituted by 4 LEDs attached on a piece of tissue needs to be miniaturized in order to better fit the size of a pig's heart. Furthermore, the way of attaching these markers to the surface of the heart must be improved. The real-time use of electrocardiogram signals is also a promising way of improvement.

ACKNOWLEDGMENT

This work was supported by an "ACI jeunes chercheurs" funding from the French government. Some experiments are performed on an AESOP robot that has been graciously provided by Computer Motion Inc.

REFERENCES

[1] P. F. Gründeman, C. Borst, and E. W. L. Jansen, "Coronary artery bypass grafting without cardiopulmonary bypass: the utrecht "octopus" tissue stabilizer," *Kardiol Pol, Polish Society of Cardiology*, vol. 52, pp. 43–46, 2000.

[2] T. Gilhuly, S. Salcudean, K. Ashe, S. Lichtenstein, and P. Lawrence, "Stabilizer and surgical arm design for cardiac surgery," in *Proc. of the IEEE International Conference on Robotics and Automation*, vol. 1, May 1998, pp. 699–704.

[3] M. A. Clifford, F. Banovac, E. Levy, and K. Cleary, "Assessment of hepatic motion secondary to respiration for computer assisted interventions," *Computer Aided Surgery*, vol. 7, no. 5, pp. 291–299, 2002.

[4] T. J. Ortmaier, "Motion compensation in minimally invasive robotic surgery," Ph.D. dissertation, Technische Universität München, 2003, http://tumb1.biblio.tu-muenchen.de/publ/diss/ei/2003/ortmaier.html.

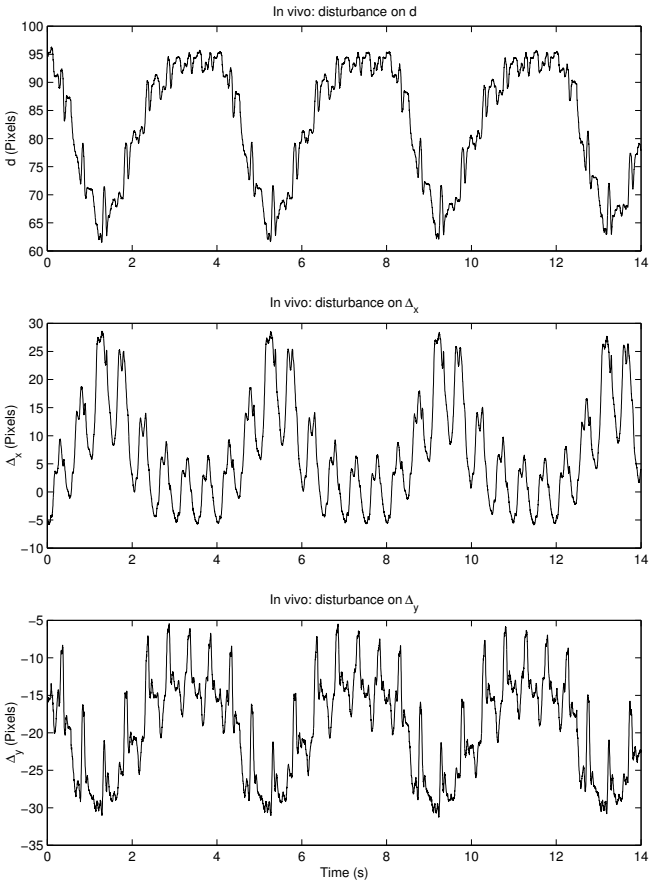

Fig. 24. *In vivo*: disturbance without compensation

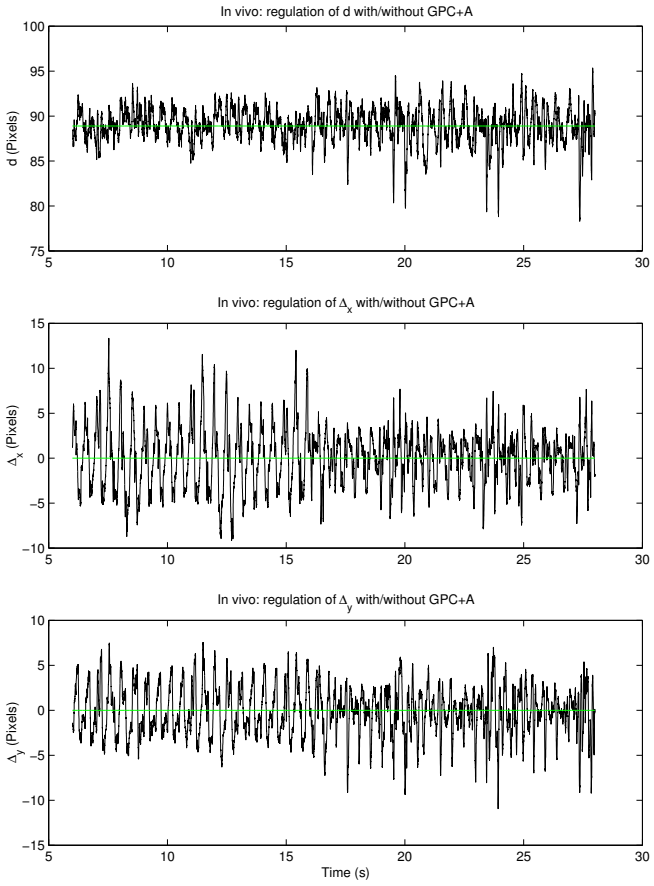

Fig. 25. *In vivo*: regulation with GPC and GPC+A (at t=16s)

[5] A. Thakral, J. Wallace, D. Tomlin, N. Seth, and N. V. Thakor, "Surgical motion adaptive robotic technology (s.m.a.r.t.): Taking the motion out of physiological motion," in *Proc. of the 4th Int. Conf. on Medical Image Computing and Computer-Assisted Intervention (MICCAI)*, Utrecht, The Netherlands, Oct. 2001, pp. 317–325.

[6] C. N. Riviere, R. S. Rader, and N. V. Thakor, "Adaptive canceling of physiological tremor for improved precision in microsurgery," *IEEE Transactions on Biomedical Engineering*, vol. 45, no. 7, pp. 839–846, 1998.

[7] C. N. Riviere, W. T. Ang, and P. K. Khosla, "Toward active tremor canceling in handheld microsirgical instruments," *IEEE Transactions on Robotics and Automation*, vol. 19, no. 5, pp. 793–800, 2003.

[8] A. Schweikard, G. Glosser, M. Bodduluri, M. Murphy, and J. Adler, "Robotic motion compensation for respiratory motion during radiosurgery," *Journal of Computed Aided Surgery*, vol. 5, no. 4, pp. 263–277, Sept. 2000.

[9] Y. Nakamura, K. Kishi, and H. Kawakami, "Heartbeat synchronization for robotic cardiac surgery," in *Proc. of the IEEE International Conference on Robotics and Automation*, Seoul, Korea, May 2001.

[10] D. W. Clarke, C. Mohtadi, and P. S. Tuffs, "Generalized predictive control - part 1. The basic algorithm," *Automatica*, vol. 23, pp. 137–160, 1987.

[11] B. Espiau, F. Chaumette, and P. Rives, "A new approach to visual servoing in robotics," *IEEE Transactions on Robotics and Automation*, vol. 8, no. 3, pp. 313–326, 1992.

[12] S. Hutchinson, G. D. Hager, and P. I. Corke, "A tutorial on visual servo control," *IEEE Transactions on Robotics and Automation*, vol. 12, no. 5, pp. 651–670, 1996.

[13] A. Krupa, J. Gangloff, C. Doignon, M. de Mathelin, G. Morel, J. Leroy, L. Soler, and J. Marescaux, "Autonomous 3-D positioning of surgical instruments in robotized laparoscopic surgery using visual servoing," *IEEE Transactions on Robotics and Automation*, vol. 19, no. 5, pp. 842–853, 2003.

[14] J. J. Craig, "Adaptive control of manipulators through repeated trials," in *Proc. of the American Control Conference*, San Diego, California, 1984, pp. 1566–1573.

[15] G.-Y. Zhu, A. Zamamiri, M. A. Henson, and M. A. Hjortsø, "Model predictive control of continuous yeast bioreactors using cell population balance models," *Chemical Engineering Science*, vol. 55, pp. 6155–6167, 2000.

[16] S. Natarajan and J. H. Lee, "Repetitive model predictive control applied to a simulated moving bed chromatography system," *Computers and Chemical Engineering*, vol. 24, pp. 1127–1133, 2000.

[17] J. H. Lee, S. Natarajan, and K. S. Lee, "A model-based predictive control approach to repetitive control of continuous processes with periodic operations," *Journal of Process Control*, vol. 11, pp. 195–207, 2001.

[18] E. F. Camacho and C. Bordons, *Model Predictive Control*. London: Springer-Verlag, 1999.

[19] E. Bianchi, L. Dozio, and P. Mantegazza, *A hard real time support for LINUX*, Dipartimento di Ingegneria Aerospaziale, Politecnico di Milano, 2002, http://www.aero.polimi.it/ rtai/documentation/index.html.

[20] J. A. Gangloff and M. F. de Mathelin, "High speed visual servoing of a 6 DOF manipulator using multivariable predictive control," *Advanced Robotics*, vol. 17, no. 10, pp. 993–1021, Dec. 2003, special issue : advanced 3D vision and its application to robotics.

[21] K. Y. Rani and H. Unbehauen, "Study of predictive controller tuning methods," *Automatica*, vol. 33, no. 12, pp. 2243–2248, 1997.

[22] M. Bodson and S. C. Douglas, "Adaptive algorithms for the rejection of sinusoidal disturbances with unknown frequency," *Automatica*, vol. 33, no. 12, pp. 2213–2221, 1997.

[23] C. Vaz, X. Kong, and N. Thakor, "An adaptive estimation of periodic signals using a fourier linear combiner," *IEEE Transactions on Signal Processing*, vol. 42, no. 1, pp. 1–10, 1994.